Proceedings of the ICBBG2025
2025 International conference on Bio-mediated and Bio-inspired Geotechnics
18-20 May, 2025 | Tempe, Arizona, USA
https://doi.org/10.53243/ICBBG2025-78

Investigation of Pullout Resistance of Geogrids with Different Topologies

Candas Oner[1], J. David Frost, Ph.D., P.E., F. ASCE[2]

[1]School of Civil & Environmental Engineering, Georgia Institute of Technology, 790 Atlantic Drive, Atlanta, GA, USA; E-mail: candasoner3@gatech.edu
[2]School of Civil & Environmental Engineering, Georgia Institute of Technology, 790 Atlantic Drive, Atlanta, GA, USA; E-mail: david.frost@ce.gatech.edu

ABSTRACT

The interaction between geogrids and geomaterials plays an important role in composite system performance. The quantification of this interaction between particles and geogrid can be investigated using interface shear testing or geogrid pullout testing. In this study, coupling of the 3D Finite Difference Method (FDM) and Discrete Element Method (DEM) was employed to simulate pullout testing. The geogrids used in this study were imported and modeled in FDM, while the distinct soil particles were modeled using DEM. After the model was generated, the effectiveness of geogrids with different topologies was compared. For different types of geogrids, changes in the pullout force with pullout displacement were determined. In addition, the total elastic work of the geogrid was recorded. Overall, it was demonstrated that the opening size and shape of the geogrids have significant importance for the soil-geogrid interaction mechanism.

INTRODUCTION

Geogrids are an effective solution in geotechnical stabilization problems and are frequently used in pavement structures, foundations, and grade separation structures such as retaining walls and embankments. The effectiveness of geogrids lies in their tensile strength and degree of compatibility with the surrounding soil. There are established tests used to determine the tensile strength of geogrids alone, including single rib tensile tests and wide width tensile tests. Other tests that are conducted to assess the interaction between the geogrid and the surrounding soil include the interface shear test and the pullout test. Among these tests, pullout testing is the only test that allows for quantification of the soil-geogrid interaction by evaluating the pullout resistance of a geogrid in a soil box in a predetermined direction.

There are several geometrical components and material components of geogrids that can influence the soil-geogrid interaction. The geometrical components include the shape, size and size distribution of the apertures, while material components include the stiffness and tensile strength of the polymer that the geogrid is made of. In the literature, there are studies that investigated the effects of the geometrical shape of the geogrid (Liu et al., 2017; Venkateswarlu et al., 2023; Zhang et al., 2021), aperture size of the geogrid (Derksen et al., 2021; Venkateswarlu et al., 2023; Wang et al., 2023), and material properties (Derksen et al., 2023; Jaiswal & Chauhan, 2021).

Bio-inspiration in geotechnical engineering is a rapidly growing field. In the literature, there are some examples of the successful implementation of bio-inspiration in geotechnical engineering. Some of those include snake-skin inspired surface applications (Gayathri & Vangla,

2024; O'Hara & Martinez, 2024), root-inspired ground anchors (Huntoon et al., 2023; Kim et al., 2024), and angel-wing inspired surfaces for drilling applications (Zhao et al., 2024).

An additional geometrical feature of geogrids that has perhaps not been so well appreciated is the effect of the number of continuous ribs. As mentioned before, there are studies that have investigated the geometrical shape of the apertures, which is primarily related to rib continuity. The number of continuous radial ribs, when increased, encompasses a wider area being stabilized. This opportunity is supported by studying spider-webs. With this understanding, spider-webs are selected as the starting point because of numerous continuous radial ribs of those structures. The first spider-web inspired geogrid design was intentionally selected as a 'complex' structure. By utilization of a structural optimization technique called mass-constrained compliance minimization, a modified version of a spider-web inspired geogrid was generated with the elimination of the unnecessary system components in the initial design. The initial design and the optimized design after the elimination of some ribs are shown in Figure 1.

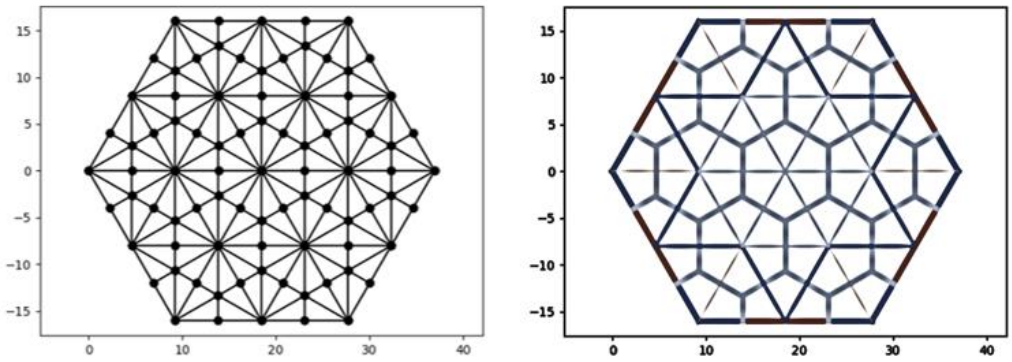

Figure 1. The initial spider-web inspired geogrid design (left) and the optimized spider-web inspired geogrid design (SpiderAx) (right).

For the present study, this optimized spider-web inspired geogrid (SpiderAx) was compared with a triaxial geogrid using FDM-DEM coupling technique to quantify their pullout resistance. The outer dimensions of both structures were generated as equal to facilitate the comparison. Both geogrid structures are illustrated in Figure 2.

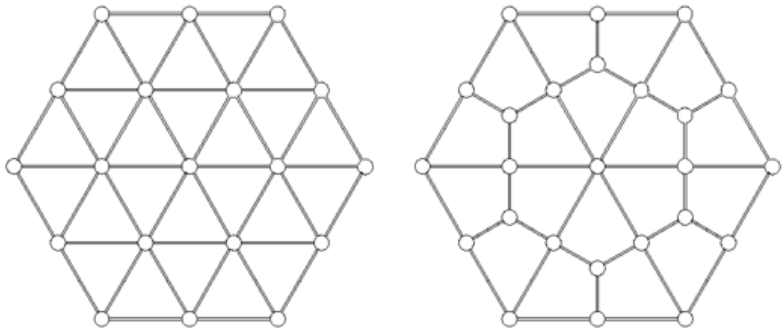

Figure 2. Triaxial geogrid used in this study (left) and SpiderAx (right).

METHODOLOGY

For this study, a coupling mechanism between FLAC3D and PFC3D was utilized. The continuum part, which is the geogrid mesh, was generated using the FLAC3D built-in mesh generator. The soil part was modelled using PFC3D clumps, and exterior walls of the model box and surcharge loading plate were generated using PFC3D walls. The detailed system generation is explained below.

The numerical model generation is divided into 6 steps:

1) *Generation of the exterior walls:* Soil particles are expected to settle under gravity. Exterior walls are generated to contain soil particles. Those walls were generated first to interact with the lower half of the soil box.
2) *Generation of the lower half of the soil box:* A cloud of soil particles consisting of clumps was generated and allowed to settle under gravity. Each clump consists of two balls, and each ball has a diameter of 1.5cm. When the clumps had settled, the top part of the lower half of the soil box was trimmed. The height of the lower half of the soil box was 10cm. The soil box dimensions were 0.4m x 0.4m x 0.2m. The half-filled soil box is illustrated in Figure 3.

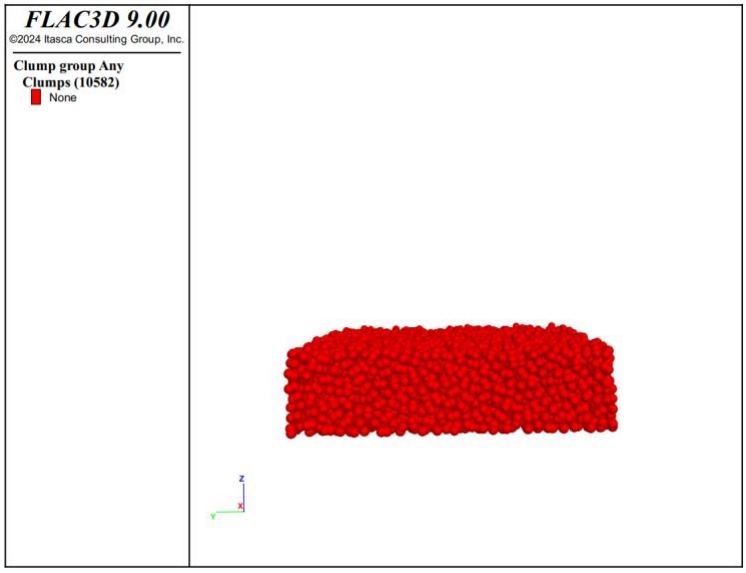

Figure 3. The half-filled soil box in FLAC3D Interface.

3) *Importing the geogrid geometry, creating the mesh of the geogrid, and enabling the wall-zone interface:* Geogrid geometries were imported at this stage with a .stl file extension from AutoCAD. After importing the geometry, the built-in mesh generator was utilized to create the mesh. Geogrid was placed 1mm above the soil box to avoid any initial contact. Then, the wall and zone coupling were activated, in which exterior surfaces of the zones were covered with PFC walls. After this stage was completed, geogrid properties were attributed to the zones, and those zones covered with walls were allowed to settle under gravity. The geogrid mesh with FLAC3D zones is illustrated in Figure 4.

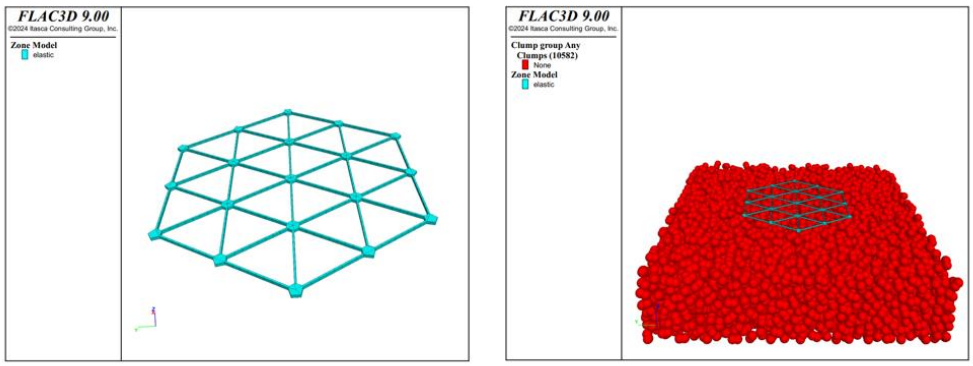

Figure 4. Geogrid mesh (left) and the location of the geogrid in the soil box (right).

4) *Generation of the top half of the soil box:* As in the case of step 2 above, a cloud of soil particles was generated and allowed to settle under gravity. After the system came to equilibrium, the top surface was trimmed. The total height of the soil box became 20cm.
5) *Generation of the surcharge loading plate and applying the surface load:* A surcharge loading plate was defined as a PFC wall, that was 2mm above the soil box to prevent any initial contact. Then, the wall servo command was activated to apply a surcharge force of 20kN. To prevent any possible system failure, the velocity of the surcharge wall was limited to 0.2m/s. All the system components before the pullout motion are shown in Figure 5.

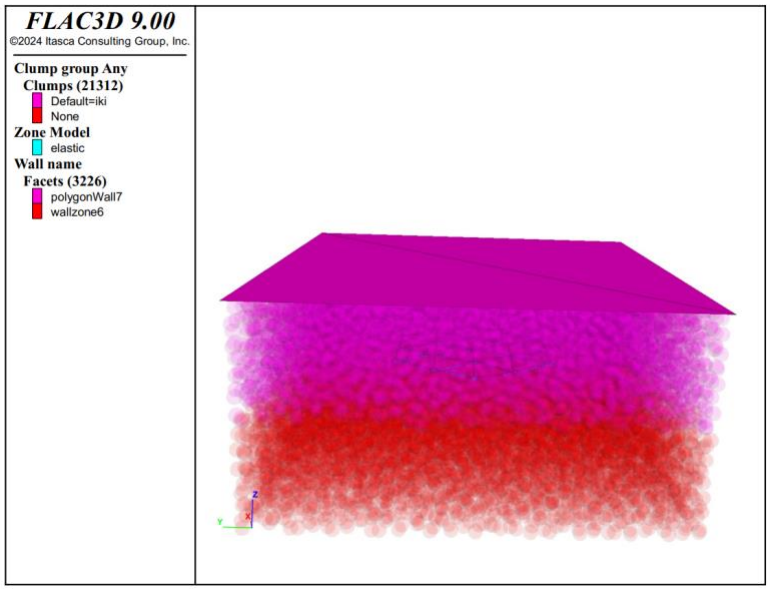

Figure 5. The top loading plate, clumps (transparent), and the geogrid mesh inside the soil box.

6) *Initiation of the pullout movement:* After the system components came to equilibrium, the velocity of the geogrid zones was initialized to move in the x-direction (horizontal) at a rate of 5mm/s. The pullout resistance was calculated from the total force on the grid points within the geogrid zones.

Using the history logic of PFC3D, the total unbalanced force was tracked during the simulation. Also, the total elastic work done in the geogrid zones was measured to quantify the geogrid 'damage' because of the pullout motion. This damage is considered as an 'artificial damage' and will be explained in the results and discussion section. These steps were repeated for two different geogrid types. Material properties and contact model properties are listed in Table 1.

Table 1. Properties used in the simulations.

	Properties	Value	Unit
Zone	Young's Modulus	250	MPa
	Poisson's Ratio	0.2	-
Contacts	***Pebble-Pebble***		
	Friction Coefficient	0.6	-
	Normal Stiffness	$1x10^8$	N/m
	Shear Stiffness	$1x10^8$	N/m
	Normal Critical Damping Ratio	0.7	-
	Pebble-Facet		
	Friction Coefficient	0.3	-
	Normal Stiffness	$1x10^8$	N/m
	Shear Stiffness	$1x10^8$	N/m

RESULTS AND DISCUSSION

A comparison between a triaxial geogrid and SpiderAx was made using the difference in their pullout capacity. Due to the computational cost, only 1.5cm of pullout displacement was simulated. The aperture size for the triaxial geogrid was 3.82cm, and the equivalent diameter for the clumps was 2cm. The difference in pullout test results is shown in Figure 6.

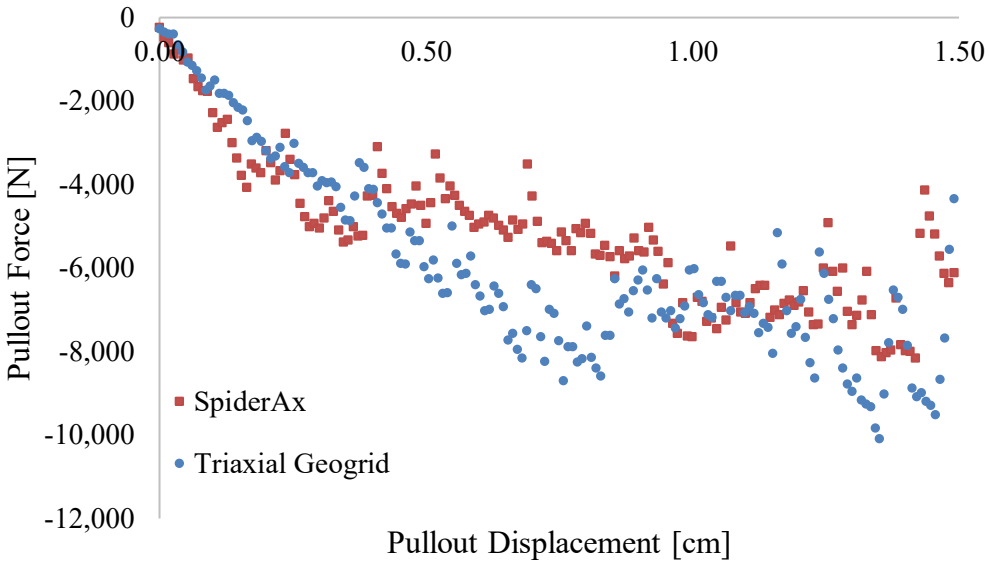

Figure 6. Pullout force vs. pullout displacement for different geogrid topologies.

As shown in Figure 6, the overall response of the SpiderAx geogrid was almost linear until approximately 0.4 cm pullout displacement. This linear type of response continued to almost 0.8cm pullout displacement for the triaxial geogrid. After about 1cm of pullout displacement, some minor fluctuations in the pullout force for both geogrids were observed with the increase in the pullout displacement. These fluctuations are hypothesized to be related to the development (making-breaking) of geogrid-aggregate resistance forces as the geogrid translates relative to the particles. The magnitude of fluctuations occurred differently for the two geogrids.

In the pullout process, because of the interaction between the soil and the geogrid, there were likely some variable distortions in geogrid shape. To begin to explore this, the total elastic work done to the geogrid zones was determined. Total elastic work done can be considered as energy absorption, meaning that when a structure deforms more, it stores more energy. This can be linked to the 'equivalent damage' that the geogrid has undergone. This is termed as equivalent, because in order to define geogrids, zones having linear elasticity were used. Therefore, this damage is not directly linked to any kind of fracture. It is a term that is used as the quantification of the absorption of the energy and how it affected the geogrid structure in this study.

The change in total elastic work for both geogrids is illustrated in Figure 7. Total elastic work includes both the volumetric and shear components of the work. At small pullout displacements, linearity of the slope for strain energy versus the pullout displacement curve remained similar for the two geogrids. However, the strain energy difference between triaxial geogrid and SpiderAx increased with further increase in the displacement, likely reflective of the different strain energy stored in the geogrids.

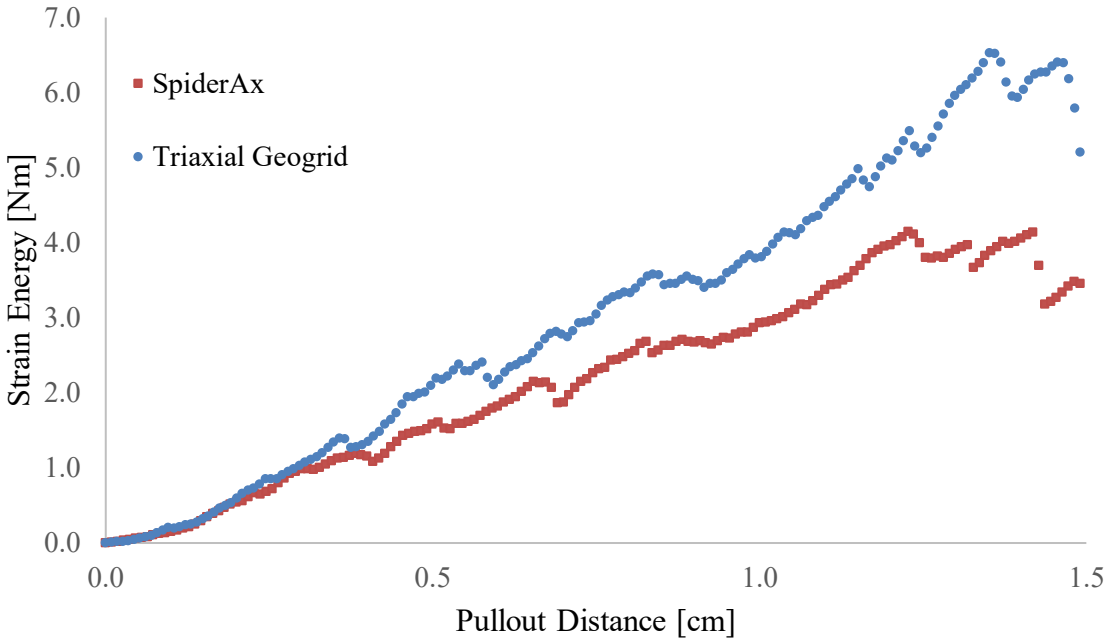

Figure 7. Total elastic energy in different geogrids.

CONCLUSION

Geometrical properties of geogrids play an important role in their interlocking behavior with surrounding soil. In this study, bio-inspiration and structural optimization techniques were used to generate a spider-web-inspired geogrid. This new design and a triaxial geogrid having the exact same unit cell outer dimensions were generated and embedded in a discrete media specimen consisting of PFC3D clumps. The effects of the different geometrical configurations were compared and discussed by evaluating their pullout resistance forces and estimated total elastic work stored in the geogrid. Based on the results of this study, the following observations are made:

- Pullout resistance and fluctuations change with different geogrid topologies. The displacement at which these fluctuations also change with the geogrid topology.
- A total elastic work parameter was defined and used as a measurement of the 'equivalent damage'. This equivalent damage increased with the pullout displacement because of the continuous interaction between the clumps and the different zones. In the investigated pullout displacement range, the total elastic work that is done on the different geogrids has shown different behavior.

LIMITATIONS AND FUTURE WORK

In this study, only one aperture size to clump diameter ratio, which is highly important for the determination of geogrid pullout resistance, was tested. Further, only one set of material properties of the geogrid zones was used. A parametric study is ongoing to understand the effects of the zone

properties on the pullout resistance and the total elastic work on the geogrid. An additional parametric study is being performed to determine the effect of the constitutive model selection on the total elastic work on the geogrid.

ACKNOWLEDGMENTS

The participation of the authors in the study reported in this manuscript was supported in part by the US National Science Foundation through the Engineering Research Center on Bio-mediated and Bio-inspired Geotechnics (CBBG). The NSF support through PTE Federal Award No. EEC-1449501 is gratefully acknowledged. The opinions in the manuscript are those of the authors and not the sponsor. The authors would like to thank the Itasca Educational Partnership (IEP) Research Program for the software loans and mentorship and Dr. David Potyondy for the associated mentorship.

REFERENCES

Derksen, J., Fuentes, R., & Ziegler, M. (2023). Geogrid-soil interaction: experimental analysis of factors influencing load transfer. *Geosynthetics International*, *30*(3), 315-336. https://doi.org/10.1680/jgein.21.00110

Derksen, J., Ziegler, M., & Fuentes, R. (2021). Geogrid-soil interaction: A new conceptual model and testing apparatus. *Geotextiles and Geomembranes*, *49*(5), 1393-1406. https://doi.org/10.1016/j.geotexmem.2021.05.011

Gayathri, V. L., & Vangla, P. (2024). Shear behaviour of snakeskin-inspired ribs and soil interfaces. *Acta Geotechnica*, *19*(3), 1397-1419. https://doi.org/10.1007/s11440-023-02009-w

Huntoon, J. A., Thomas, V. M., & Frost, J. D. (2023). Life Cycle Assessment of Root-Inspired Ground Anchors and Conventional Ground Anchors. *Geo-Congress 2023: Soil Improvement, Geoenvironmental, and Sustainability*, *339*, 1-14.

Jaiswal, S., & Chauhan, V. B. (2021). Evaluation of Optimal Design Parameters of the Geogrid Reinforced Foundation with Wraparound Ends Using Adaptive FEM. *International Journal of Geosynthetics and Ground Engineering*, *7*(4). https://doi.org/10.1007/s40891-021-00325-3

Kim, Y. A., Burrall, M., Jeon, M. K., Dejong, J. T., Martinez, A., & Kwon, T. H. (2024). Pullout behavior of tree root-inspired anchors: development of root architecture models and centrifuge tests. *Acta Geotechnica*, *19*(3), 1211-1229. https://doi.org/10.1007/s11440-023-02077-y

Liu, S. S., Huang, H., Qiu, T., & Kwon, J. (2017). Comparative Evaluation of Particle Movement in a Ballast Track Structure Stabilized with Biaxial and Multiaxial Geogrids. *Transportation Research Record*(2607), 15-23. https://doi.org/10.3141/2607-04

O'Hara, K. B., & Martinez, A. (2024). Cyclic axial response and stability of snakeskin-inspired piles in sand. *Acta Geotechnica*, *19*(3), 1139-1158. https://doi.org/10.1007/s11440-023-02007-y

Venkateswarlu, H., SaiKumar, A., & Latha, G. M. (2023). Sand-geogrid interfacial shear response revisited through additive manufacturing. *Geotextiles and Geomembranes*, *51*(4), 95-107. https://doi.org/10.1016/j.geotexmem.2023.04.001

Wang, H., Kang, M. G., Qamhia, I. I. A., Tutumluer, E., Wayne, M. H., & Shoup, H. (2023). Evaluation of Open-Graded Aggregates Stabilized with a Multi-Axial Geogrid Using a Large-Scale Triaxial Test Set-Up. *Transportation Research Record*, *2677*(10), 339-350. https://doi.org/10.1177/03611981231161351

Zhang, J., Cao, W. Z., & Zhou, Y. J. (2021). Mechanical Behavior of Triaxial Geogrid Used for Reinforced Soil Structures. *Advances in Civil Engineering*, *2021*. https://doi.org/10.1155/2021/5598987

Zhao, Y. M., Deng, B. Z., Cortes, D. D., & Dai, S. (2024). Morphological advantages of angelwing shells in mechanical boring. *Acta Geotechnica*, *19*(3), 1179-1190. https://doi.org/10.1007/s11440-023-01962-w